J|A|C|S
ARTICLES
Published on Web 06/14/2006

PNA/dsDNA Complexes: Site Specific Binding and dsDNA Biosensor Applications

Erin Shammel Baker,[†] Janice W. Hong,[†] Brent S. Gaylord,[‡] Guillermo C. Bazan,*[,†,‡] and Michael T. Bowers*[,†]

Contribution from the Department of Chemistry & Biochemistry, Department of Materials, Center for Polymers and Organic Solids, University of California, Santa Barbara, California 93106

Received January 4, 2006; E-mail: bazan@chem.ucsb.edu, bowers@chem.ucsb.edu

Abstract: The ability of peptide nucleic acids (PNA) to form specific higher-order (i.e., three- and four-stranded) complexes with DNA makes it an ideal structural probe for designing strand-specific dsDNA biosensors. Higher-order complexes are formed between a dye-labeled charge-neutral PNA probe and complementary dsDNA. Addition of a light-harvesting cationic conjugated polymer (CCP) yields supramolecular structures held together by electrostatic forces that incorporate the CCP and the dye-labeled PNA/DNA complexes. Optimization of optical properties allows for excitation of the CCP and subsequent fluorescence resonance energy transfer (FRET) to the PNA-bound dye. In the case of noncomplementary dsDNA, complexation between the probe and target does not occur, and dye emission is weak. The binding between PNA and noncomplementary and complementary dsDNA was examined by several methods. Gel electrophoresis confirms specificity of binding and the formation of higher-order complexes. Nano-electrospray mass spectrometry gives insight into the stoichiometric composition, including PNA/DNA, PNA_2/DNA, PNA/DNA_2, and PNA_2/DNA_2 complexes. Finally, structural characteristics and binding-site specificity were examined using ion mobility mass spectrometry in conjunction with molecular dynamics. These results give possible conformations for each of the higher-order complexes formed and show exclusive binding of PNA to the complementary stretch of DNA for all PNA/DNA complexes. Overall, the capability and specificity of binding indicates that the CCP/PNA assay is a feasible detection method for dsDNA and eliminates the need for thermal denaturing steps typically required for DNA hybridization probe assays.

Introduction

The stability and specificity of Watson−Crick (WC) base pairing in nucleic acids is nature's elegant way to achieve molecular recognition and in turn allow genetic information to be stored, transferred, and expressed in living systems.[1] Structural adaptation of synthetic oligonucleotides gives rise to a range of versatile recognition elements based on WC base pairing for strand-specific DNA detection. In peptide nucleic acid (PNA) analogues standard DNA nucleobases are incorporated into an altered backbone, where the sugar−phosphate backbone of DNA is replaced by a polyamide structure composed of *N*-(2-aminoethyl)glycine units and the nucleobases are attached with methylenecarbonyl linkers.[2,3] A schematic comparison of a PNA and DNA backbone is shown in Scheme 1. A key feature of PNA is the absence of negatively charged phosphate groups, which eliminates the Coulombic repulsion that occurs in natural nucleic acid hybridization. As such, DNA and RNA tend to bind to PNA strands more tightly than to each other,[4,5] and more readily form higher-order PNA/double-stranded DNA (dsDNA) complexes.[6] PNA has also been found to be stable toward nuclease, protease, and peptidase activity, indicating that it is more robust in cells than DNA, RNA, and proteins.[7] Such features make PNA an excellent candidate for molecular recognition in biosensor design.

Scheme 1. Structural Differences between a PNA and DNA Backbone

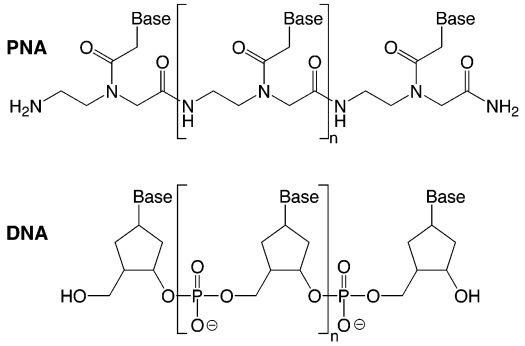

[†] Department of Chemistry & Biochemistry.
[‡] Department of Materials.

(1) Sinden, R. R. *DNA Structure and Function*; Academic Press: San Diego, 1994.
(2) Nielsen, P. E.; Egholm, M. *Peptide Nucleic Acids: Protocols and Applications*; Horizon Scientific Press: Portland, 1999.
(3) Stender, H.; Fiandaca, M.; Hyldig-Nielsen, J. J.; Coull, J. *J. Microbiol. Methods* **2002**, *48*, 1.
(4) Egholm, M.; Buchardt, O.; Christensen, L.; Behrens, C.; Freier, S. M.; Driver, D. A.; Berg, R. H.; Kim, S. K.; Norden, B.; Nielsen, P. E. *Nature* **1993**, *365*, 566.
(5) Maher, L. J.; Wold, B.; Dervan, P. B. *Science* **1989**, *245*, 725.
(6) Nielsen, P. E.; Egholm, M.; Bèrg, R. H.; Buchardt, O. *Science*, **1991**, *254*, 1497.

10.1021/ja060069s CCC: $33.50

Scheme 2. dsDNA Detection Using a Cationic Conjugated Polymer (CCP, shown in blue) and a Specific PNA-C* Optical Reporter Probe (shown in black)[a]

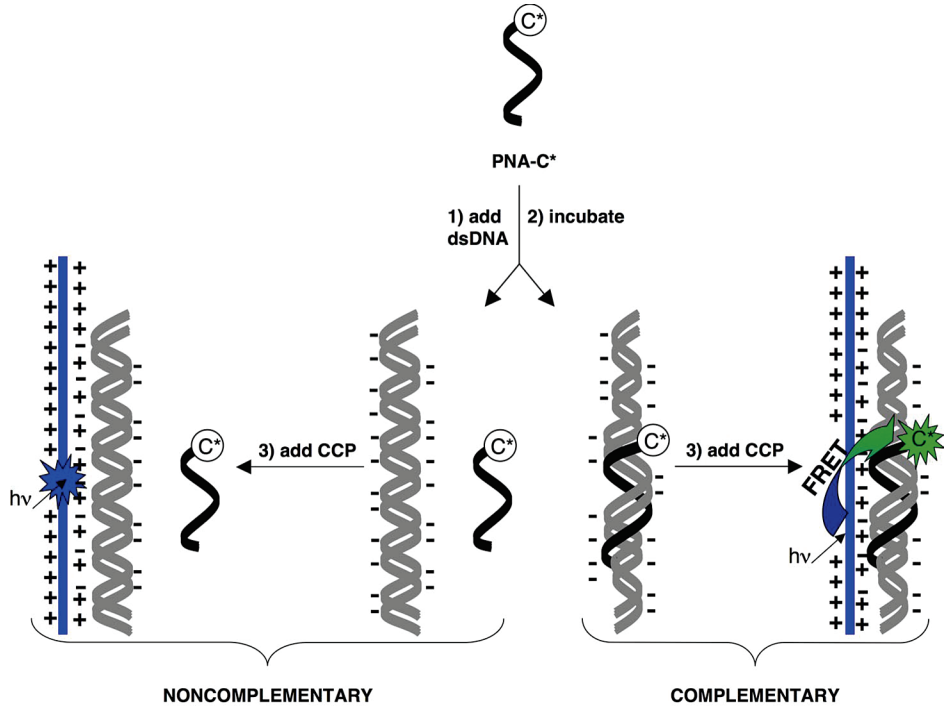

[a] PNA-C* is noncomplementary to the dsDNA on the left and complementary to dsDNA on the right.

Conventional nucleic acid recognition probes[8−11] rely on a specific hybridization event to indicate the presence of a particular target sequence. However, since DNA is rarely present as single-strands (naturally or reproduced by PCR), a thermal denaturing step is typically required to separate the target duplex into two (single) strands, thus allowing for probe hybridization. The sensitivity of these probe assays is dependent on the competition between probe hybridization and duplex reannealing.[12−14] Conventional PCR exponentially amplifies the target, leading to higher copy numbers. However, these targets are double-stranded, leading to problems with competitive hybridization. Despite the fact that asymmetric PCR produces fewer targets (linear growth), it is possible to generate higher signals because only one strand of the target is copied, resulting in single-stranded product, eliminating the possibility of target reannealing prior to probe hybridization.[8,12] These considerations highlight the importance of developing assays that can probe dsDNA directly without the need for thermal melting and competitive reannealing.[15,16]

The development of homogeneous biosensors based on PNA recognition has recently received much attention.[17−19] In particular, biosensors based on fluorescence resonance energy transfer (FRET) utilizing cationic conjugated polymer (CCP) donors and dye-labeled PNA acceptors (PNA-C*) have shown promise as highly sensitive hybridization assays. In such assays, electrostatic attraction brings the CCP and anionic DNA into close proximity. If the ssDNA target hybridizes to a complementary PNA-C* probe, the donor (CCP) and acceptor (C*) are close enough that excitation of the CCP results in FRET and emission from C*. If the target is not complementary to the PNA probe, the polymer to C* distance is large, and no C* emission is observed.

PNA was originally developed as a binding agent for dsDNA,[6] and it has shown positive results in analogous ssDNA sensors.[20,21] A biosensor mechanism for dsDNA based on PNA/dsDNA recognition properties and the action of a cationic conjugated polymer is depicted in Scheme 2. In this process, the emission of the donor or acceptor would signify the absence or presence of the target, respectively.

While the combination of a dsDNA and a complementary ssPNA may seem straightforward, multiple binding modes are possible. Understanding the structure of these higher-order PNA/DNA complexes and the conditions in which they occur is required for rational development and design of dsDNA detection methods. A common method to study these complexes is the electrophoretic mobility shift assay (EMSA), in which a comparison is made between the band shifts arising from dsDNA and other higher-order complexes. Because the mobility of these bands is dependent on the interplay of the charge density

(7) Demidov, V. V.; Potaman, V. N.; Frank-Kamenetskii, M. D.; Egholm. M.; Buchard, O.; Sönnichsen, S. H.; Nielsen, P. E. *Biochem. Pharmacol.* **1994**, *48*, 1310.
(8) Tyagi, S.; Kramer, F. R. *Nat. Biotechnol.* **1996**, *14*, 303.
(9) Holland, P. M.; Abramson, R. D.; Watson, R.; Gelfand, D. H. *Proc. Natl. Acad. Sci. U.S.A.* **1991**, *88*, 7276.
(10) Thelwell, N.; Millington, S.; Solinas, A.; Booth, J.; Brown, T. *Nucleic Acids Res.* **2000**, *28*, 3752.
(11) Wittwer, C. T.; Herrmann, M. G.; Moss, A. A.; Rasmussen, R. P. *Biotechniques*, **1997**, *22*, 130.
(12) Poddar, S. K. *Mol. Cell. Probes* **2000**, *14*, 25.
(13) Sanchez, J. A.; Pierce, K. E.; Rice, J. E.; Wangh, L. J. *Proc. Natl. Acad. Sci. U.S.A.* **2004**, *101*, 1933.
(14) Wei, Q.; Liu, S.; Huang, J.; Mao, X.; Chu, X.; Wang, Y.; Qiu, M.; Mao, Y.; Xie, Y.; Li, Y. *J. Biochem. Mol. Biol.* **2004**, *37*, 439.
(15) Gorelov, V. N.; Roher, H.-D.; Goretzki, P. E. *Biochem. Biophys. Res. Commun.* **1994**, *200*, 365.
(16) Drewe, L. J.; Brightwell, G.; Hall, E. A. H. *Mol. Cell. Probes* **2000**, *14*, 269.
(17) Maxwell, D. J.; Taylor, J. R.; Nie, S. M. *J. Am. Chem. Soc.* **2002**, *124*, 9606.
(18) Gaylord, B. S.; Heeger, A. J.; Bazan, G. C. *J. Am. Chem. Soc.* **2003**, *125*, 896.
(19) Liu, B.; Bazan, G. C. *Chem. Mater.* **2004**, *16*, 4467.
(20) Gaylord, B. S.; Heeger, A. J.; Bazan, G. C. *Proc. Natl. Acad. Sci. U.S.A.* **2002**, *99*, 10954.
(21) Liu, B.; Bazan, G. C. *Proc. Natl. Acad. Sci. USA* **2005**, *102*, 589.

Scheme 3. Structures of the O-Linker and PFP

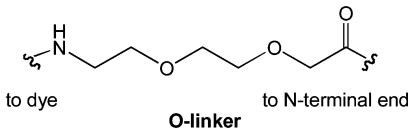

O-linker

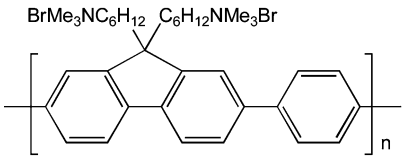

PFP

and the size/conformation of the complex, band shifts are difficult to predict, and subsequent conclusions are qualitative in nature. Alternatively, the product represented by these bands can be analyzed by mass spectrometry. Electrospray ionization mass spectrometry (ESI-MS) allows all of the noncovalently bound complexes in a solution to be studied simultaneously,[22−26] and with the aid of ion mobility methods and molecular dynamics calculations,[27,28] conformational information about these complexes can also be acquired. Recently, ESI-MS in conjunction with ion mobility methods, indicated that DNA helices[29,30] and G-quadruplexes[31−33] are stable without solvent and retain most of their solution-phase characteristics. From these results, it appears that this method is ideal for analyzing noncovalently bound PNA/DNA complexes.

In this contribution, we demonstrate a homogeneous FRET-based biosensor composed of a CCP and a dye-labeled PNA probe for the detection of sequence-specific dsDNA. Additionally, we provide a detailed structural investigation into the types of complexes formed between a PNA strand and different dsDNA structures. By analyzing results obtained from FRET experiments, gel electrophoresis, and ion mobility mass spectrometry, we can obtain insight into the mechanism of the dsDNA detection scheme.

Experimental Section

Materials. The HPLC-purified PNA sequence, Fl-OO-$(TC)_5$ (named P-Fl), was purchased from Applied Biosystems (Foster City, CA) and used without further purification. The PNA was labeled with fluorescein at the N-terminal end using two O-linkers (Scheme 3) for the FRET experiments. The linkers prevent the fluorescein from interfering with base pairing and reduce quenching of the dye by the bases. Four different 30-base DNA sequences were purchased from Integrated DNA Technologies, Inc. (Coralville, IA) and used without further purification. Two of the DNA sequences, C_A (GAG CTC GGT A$(TC)_5$A GTC GAA TCG) and C_B (CGA TTC GAC T$(GA)_5$T ACC GAG CTC), were designed to be complementary to each other with C_B also having a 10-base stretch complementary to the PNA strand. The other two sequences, N_A (CTG TTG CAC TAT GCC AGA CAA TAA TTT TCT) and N_B (AGA AAA TTA TTG TCT GGC ATA GTG CAA CAG), were designed to be complementary to each other, but noncomplementary to the PNA probe strand. The synthesis of poly[9,9-bis(6′-[*N*,*N*,*N*-trimethylammonium]hexyl)fluorene-*co*-phenylene dibromide] (PFP) (Scheme 3) has been reported previously.[34]

PNA/DNA Sample Preparation. Duplex DNA (N_A/N_B and C_A/C_B) was annealed at a concentration of 10 μM in 4 mM ammonium acetate buffer (pH 6.6) by heating to 85 °C for 10 min and then cooling overnight at room temperature. These solutions were diluted to 2 μM, and PNA was added in various amounts. These samples were incubated at 37 °C for 1 h and then cooled to room temperature.

FRET Experiments. Fluorescence spectra were recorded on a PTI QuantaMaster spectrometer with a xenon lamp at a detection angle of 90°. Photoluminescence (PL) experiments were carried out in 4 mM ammonium acetate buffer (pH 7.6). After excitation at 380 nm (the λ_{max} of the donor), PL spectra were recorded from 390 to 700 nm for the DNA/PNA samples (1.0×10^{-8} M) in the absence of the donor and after each addition of the PFP (1.0×10^{-8} M in repeat units). FRET efficiency was monitored by the intensity of the fluorescein band from 500 to 700 nm.

Gel Electrophoresis. Analysis by electrophoresis was carried out under nondenaturing conditions on 20% polyacrylamide gels, cast and run in 1 × TBE buffer at room temperature. Gels were aged overnight to ensure complete polymerization and were electrophoresed for 30 min prior to loading 15 μL of each sample (3.7×10^{-10} M DNA) into the centermost lanes. Electrophoresis was carried out at a constant power of 15 W for 2 h. Gels were stained for 45 min with a SybrGold staining solution (Invitrogen, Carlsbad, CA), chosen for its ability to stain both ssDNA and dsDNA. Images were obtained by excitation at 302 nm by the use of a UVP EPI-Chemi Darkroom (Upland, CA).

Mass Spectra and Ion Mobility Experiments. The details concerning the experimental setup for the mass spectra and ion mobility measurements have been published previously,[35] so only a brief description will be given. Approximately 6 mL of the annealed 2 μM solution was placed in a metalized glass needle (spray tip). Ions were formed by nano-ESI and injected into a specially designed ion funnel. The ions are then gently injected into a 4.5-cm long drift cell filled with ~5 Torr of helium gas and pulled at a constant drift velocity by a weak, uniform electric field applied across the cell. After exiting the drift cell, the ions are mass analyzed in a quadrupole mass filter, which can either be set for the acquisition of a mass spectrum or to detect one specific *m*/*z* as a function of time, yielding an arrival time distribution (ATD). The reduced mobility, K_o, of the mass-selected ion can be obtained from a series of ATDs measured at different electric field strengths (10−23 V/cm) using eq 1[36]

$$K_o = \left(l^2 \cdot \frac{273}{760T} \cdot \frac{p}{V} \cdot \frac{1}{t_A - t_o} \right) \quad (1)$$

where l is the length of the cell, T is the temperature in Kelvin, p is the pressure of the He gas (in Torr), V is the voltage applied to the drift cell, t_A is the ions' arrival time taken from the center of the ATD peak and t_o is the time the ion spends outside the drift cell before reaching the detector. A plot of t_A versus p/V yields a straight line with a slope inversely proportional to K_o and an intercept of t_o. K_o can be converted

(22) Whitehouse, C. M.; Dreyer, R. N.; Yamashita, M.; Fenn, J. B. *Anal. Chem.* **1985**, *57*, 675.
(23) Yamashita, M.; Fenn, J. B. *J. Phys. Chem.* **1984**, *88*, 4671.
(24) Henry, K. D.; Williams, E. R.; Wang, B.-H.; McLafferty, F. W.; Shabanowitz, J.; Hunt, D. F. *Proc. Natl. Acad. Sci. U.S.A.* **1989**, *86*, 9075.
(25) Henry, K. D.; Quinn, J. P.; McLafferty, F. W. *J. Am. Chem. Soc.* **1991**, *113*, 5447.
(26) Chowdhury, S. K.; Eshraghi, J.; Wolfe, H.; Forde, D.; Hlavac, A. G.; Johnston, D. J. *Anal. Chem.* **1995**, *67*, 390.
(27) Bowers, M. T.; Kemper, P. R.; von Helden, G.; van Koppen, P. A. M. *Science* **1993**, *260*, 1446.
(28) Clemmer, D. E.; Jarrold, M. F. *J. Mass Spectrom.* **1997**, *32*, 577.
(29) Gidden, J.; Ferzoco, A.; Baker, E. S.; Bowers, M. T. *J. Am. Chem. Soc.* **2004**, *126*, 15132.
(30) Gidden, J.; Baker, E. S.; Ferzoco, A.; Bowers, M. T. *Int. J. Mass Spectrom.* **2005**, *240*, 183.
(31) Baker, E. S.; Bernstein, S. L.; Bowers, M. T. *J. Am. Soc. Mass Spectrom.* **2005**, *16*, 989.
(32) Baker, E. S.; Lee, J. T.; Sessler, J. L.; Bowers, M. T. *J. Am. Chem. Soc.* **2006**, *128*, 2641.
(33) Baker, E. S.; Bernstein, S. L.; Gabelica, V.; De Pauw, E.; Bowers, M. T. *Int. J. Mass Spectrom.* **2006**. In press.
(34) Wang, S.; Liu, B.; Gaylord, B. S.; Bazan, G. C. *Adv. Funct. Mater.* **2003**, *13*, 463.
(35) Wyttenbach, T.; Kemper, P. R.; Bowers, M. T. *Int. J. Mass Spectrom.* **2001**, *212*, 13.
(36) Mason, E. A.; McDaniel, E. W. *Transport Properties of Ions in Gases*; Wiley: New York, 1988.

to a collision cross section, σ, using eq 2

$$\sigma = \frac{3z}{16N_o}\left(\frac{2\pi}{\mu k_b T}\right)^{1/2}\frac{1}{K_o} \quad (2)$$

where z is the charge of the ion, N_o is the number density of He at STP, T is temperature, k_b is the Boltzmann constant and μ is the ion-He reduced mass.[36]

Theoretical Modeling. Structural information can be obtained from the ion mobility results by comparing the experimental cross sections to cross sections of theoretical structures obtained from molecular dynamics modeling.[29−33] Starting structures for each PNA/DNA complex were generated from specifically bound NMR and X-ray structures. Nonspecifically bound complexes were also modeled to ensure that P-Fl is actually binding to its complementary region of C_B. The starting backbone geometry for the specifically bound PNA/DNA duplex and the PNA/DNA_2 duplex invasion structure (Scheme 4) were created using the X-ray diffraction structure 1PNN[37,38] and edited with HyperChem[39] to reflect the correct bases of the PNA and DNA sequences examined. The triplex regions in the PNA_2/DNA triplex, PNA/DNA_2 triplex, and PNA_2/DNA triplex invasion structures (Scheme 4) were created from the DNA triplex NMR structure 1AT4[38,40] and edited with HyperChem to change the DNA backbone(s) to PNA backbone(s). To generate nonspecific complexes, P-Fl was placed next to different noncomplementary regions of C_B or C_A/C_B (depending on the complex) allowing only a few WC or Hoogsteen pairs to form, in addition to many nonspecific hydrogen bonds. Molecular dynamics simulations (300 K) were run on each complex for 2 ns using the AMBER 7[41] set of programs, and every 5 ps a structure was saved. Each structure was then energy minimized and its cross section calculated. Collision cross sections for ions with more than 200 atoms were calculated using hard-sphere scattering trajectory models developed by the Jarrold group.[42,43] From the calculations for the PNA/DNA complexes, it was observed that the starting structures eventually converge to give at least one steady-state structure in which the cross section remains relatively constant. The average cross section of the final 50−100 structures in each steady state were used for comparison with the experimental values.

The experimentally observed charge states of the complexes can be readily identified from the mass spectra, but the exact locations of the deprotonation sites required for modeling are not known. Thus, the deprotonation sites on the DNA were divided and dispersed among the strands, with at least one neutral phosphate group between every deprotonated group.[44−48] Multiple DNA/PNA structures were modeled with many different deprotonation sites, but no theoretical differences in cross section or conformation were observed as a function of charge location, consistent with previously published data on dsDNA complexes.[29,30,49]

Results and Discussion

FRET Experiments. The FRET-based biosensor for dsDNA detection shown in Scheme 2 was constructed using the CCP poly[9,9-bis(6′-[*N*,*N*,*N*-trimethylammonium]hexyl)fluorene-*co*-phenylene dibromide] (PFP) as the donor and a fluorescein (Fl)-labeled homopyrimidine PNA acceptor probe (P-Fl)[50] with the 10-base sequence $(TC)_5$. For the purpose of this study, two 30 base pair (bp) dsDNA sequences were chosen. One dsDNA (N_A/N_B) was noncomplementary to P-Fl, whereas the other (C_A/C_B) was designed to have a region complementary to P-Fl. A central binding region was selected to eliminate "fraying" effects near the ends of the duplex. Each dsDNA was incubated with P-Fl at 37 °C for 1 h. PFP was then added, and side-by-side FRET comparisons of P-Fl/N_A/N_B and P-Fl/C_A/C_B were made. Fluorescence spectra were collected by excitation at 380 nm.

P-Fl to C_A/C_B ratios of 2.5:1, 7.5:1, and 15:1 were first examined. The most efficient FRET was found for the highest P-Fl:C_A/C_B ratio,[51] so a solution of 15:1 P-Fl to N_A/N_B was subsequently tested for FRET response (Figure 1). Weak fluorescein emission was observed for the noncomplementary situation, which indicates some degree of FRET, but it is not clear whether this is evidence for nonspecific higher-order complexation or merely hydrophobic interactions between PFP and P-Fl that bring them into close proximity. The fluorescein emission observed with the complementary P-Fl/C_A/C_B combination is significantly more intense, consistent with the action described in Scheme 2. However, the fluorescence spectra do not provide definitive structural information about the P-Fl and the dsDNA complexes; as a result, further analysis by gel electrophoresis, mass spectrometry, and ion mobility methods was undertaken.

Gel Electrophoresis. Figure 2 shows the image obtained from gel electrophoresis of the products obtained from P-Fl/dsDNA mixtures. The first three lanes show C_A, C_B, and C_A/C_B, respectively. Lane 4 illustrates the duplex formed when P-Fl and C_B are combined. An interesting observation is that the P-Fl/C_B duplex migrates at approximately the same rate as the C_A/C_B DNA duplex. While the P-Fl/C_B duplex has a smaller size than the C_A/C_B duplex, it also has a smaller overall charge, resulting in a similar migration rate to the C_A/C_B duplex.

Lanes 5−8 correspond to the addition of P-Fl to N_A/N_B (lane 5) and to C_A/C_B (lanes 6−8). When P-Fl is added to N_A/N_B, only bands representing P-Fl and N_A/N_B are observed. However, a new product can be detected in lanes 6−8 that show the result of increasing the ratio of P-Fl to C_A/C_B. The new band has the slowest migration rate and intensifies with increased P-Fl loading. The band for C_A also intensifies with increasing P-Fl concentration, and because C_A has a sequence similar to that of P-Fl, the faint reappearance of the C_A band indicates that it is released upon formation of P-Fl/C_B or $(P\text{-Fl})_2/C_B$ complexes. The slower migration rate of the new band and the reappearance of the C_A band suggest a three-strand complex, at least partially composed of $(P\text{-Fl})_2/C_B$.

Structural identification of the P-Fl/C_A/C_B product(s) is not feasible when relying only on the information from fluorescence spectroscopy and gel electrophoresis. In general terms, the specific binding modes of a ssPNA and complementary dsDNA can include any of the different complexes in Scheme 4.[5,6,37,52−57] A PNA_2/DNA triplex (Scheme 4a)[5,52] occurs when

(37) Betts, L.; Josey, J. A.; Veal, J. M.; Jordan, S. R. *Science* **1995**, *270*, 1838.
(38) Berman, H. M.; Westbrook, J.; Feng, Z.; Gilliland, G.; Bhat, T. N.; Weissig, H.; Shindyalov, I. N.; Bourne, P. E. *Nucleic Acids Res.* **2000**, 28, 235.
(39) *Hyperchem 7.0*; Hypercube Inc., 2002.
(40) Bartley, J. P.; Brown, T.; Lane, A. N. *Biochemistry* **1997**, *36*, 14502.
(41) Case, D. A.; et al. *AMBER 7*; University of California: San Francisco, 2002.
(42) Mesleh, M. F.; Hunter, J. M.; Shvartsburg, A. A.; Schatz, G. C.; Jarrold, M. F. *J. Phys. Chem.* **1996**, *100*, 16082.
(43) Shvartsburg, A. A.; Jarrold, M. F. *Chem. Phys. Lett.* **1996**, *261*, 86.
(44) Schnier, P. D.; Klassen, J. S.; Strittmatter, E. F.; Williams, E. R. *J. Am. Chem. Soc.* **1998**, *120*, 9605.
(45) Gabelica, V.; De Pauw, E. *J. Mass Spectrom.* **2001**, *36*, 397.
(46) Gabelica, V.; Rosu, F.; Houssier, C.; De Pauw, E. *Rapid. Commun. Mass Spectrom.* **2000**, *14*, 464.
(47) Gabelica, V.; De Pauw, E. *Int. J. Mass Spectrom.* **2002**, 219, 151.
(48) Hoaglund, C. S.; Liu, Y.; Ellington, A. D.; Pagel, M.; Clemmer, D. E. *J. Am. Chem. Soc.* **1997**, *119*, 9051.
(49) Rueda, M.; Kalko, S. G.; Luque, F. J.; Orozco, M. *J. Am. Chem. Soc.* **2003,** *125*, 8007.
(50) An evaluation of how a single CCP can be used to sensitize two fluorophores of differing acceptor frequencies can be found in Liu, B.; Bazan, G. C. *J. Am. Chem. Soc.* **2006**, *128*, 1188.
(51) The 15:1 ratio showed the best response. Data for the other ratios can be found in Supporting Information.

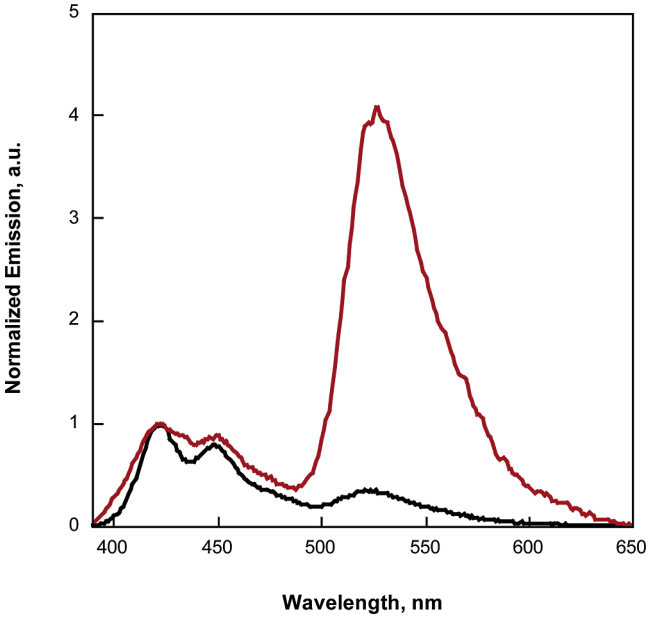

Figure 1. Fluorescence spectra of PFP (5.0×10^{-7} M repeat units) and P-Fl in the presence of N_A/N_B (black, 1.0×10^{-8} M DNA) and C_A/C_B (red 1.0×10^{-8} M DNA) by excitation of the conjugated polymer PFP at 380 nm. The spectra are normalized relative to the PFP emission.

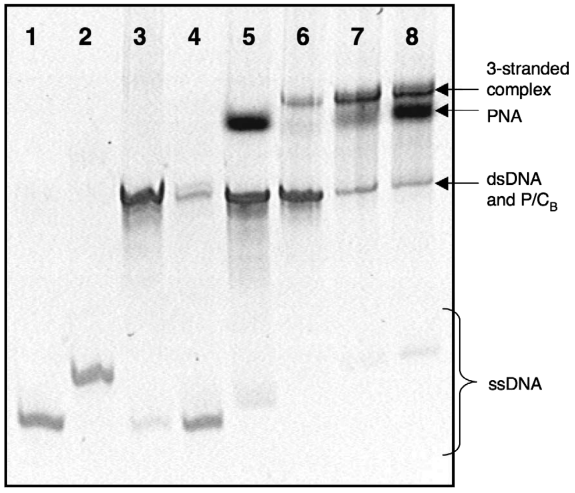

Figure 2. Polyacrylamide gel electrophoresis analysis. Lanes 1 and 2 illustrate C_B and C_A alone, 3 is the C_A/C_B duplex, 4* shows P-Fl combined with only C_B, 5 is P-Fl combined with N_A/N_B at a 15 to 1 ratio, and 6−8 show P-Fl combined with C_A/C_B in different ratios: lane 6 is 2.5:1 ratio; lane 7 is 7.5:1 ratio; lane 8 is 15:1 ratio. *In lane 4, the ratio of P-Fl:C_B is 2:3.

one ssPNA WC pairs to its complementary DNA strand while another ssPNA binds via Hoogsteen pairing to the same DNA strand. PNA/DNA_2 complexes can form as either a standard triplex or duplex invasion. For a PNA/DNA_2 triplex (Scheme 4b), the ssPNA binds via Hoogsteen pairing to the complementary DNA strand in the major groove of the DNA duplex.[55−57]

Scheme 4. Possible PNA/DNA Complexes for One PNA Sequence and the Two Different DNA Strands in a DNA Duplex, Where Only One Strand Has a Region Complementary to the PNA

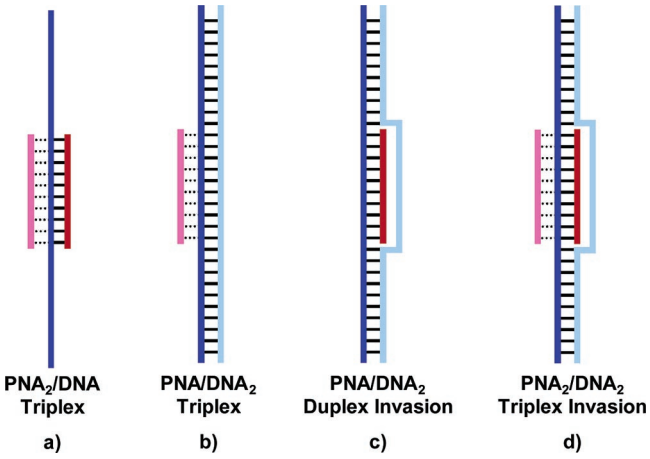

[a] The DNA strand complementary to the PNA is dark blue, the other DNA strand is light blue, Hoogsteen bound PNA is pink, and WC paired PNA is red. WC H-bonds are shown as solid lines and Hoogsteen H-bonds are shown as dotted lines.

Alternatively, PNA/DNA_2 duplex invasion (Scheme 4c) occurs when the ssPNA breaks WC pairs between the dsDNA and WC pairs to the complementary DNA strand, while the unpaired DNA strand forms a stable displacement loop (D-loop).[6,55−58] In PNA_2/DNA_2 triplex invasion (Scheme 4d), one ssPNA breaks the WC pairs of the dsDNA, and WC binds to its complementary DNA strand while another ssPNA binds via Hoogsteen pairing to the same DNA strand while the unbound DNA strand forms a D-loop around the triplex.[59]

The mechanism in Scheme 2 is therefore a simplification of the possible outcomes from P-Fl/dsDNA interactions. Nonetheless, its function should remain operative with the formation of one (or more) of these complexes. The specific formation of these structures is highly sequence dependent. For example, homopyrimidine PNA has been shown to displace the homopyrimidine strand of dsDNA to form PNA_2/DNA triplexes,[60,61] whereas homopurine PNA sequences tend to form PNA/DNA_2 duplex invasion complexes.[59] The appearance of the new band in the gel corroborates specific binding between the P-Fl and C_B or C_A/C_B and could be due to any of the complexes described in Scheme 4. The slow migration rate of the band implies the presence of higher-order complexes; however, it provides little additional information.

Mass Spectra. Mass spectrometry was used to obtain insight into the possible components in the slow-migrating gel electrophoresis band. The nano-ESI mass spectrum of P-Fl in a 15 to 1 excess over the noncomplementary 30 bp DNA duplex, N_A/N_B, is shown in Figure 3a. In this spectrum, multiple charge states of P-Fl, N_A, N_B, and N_A/N_B are observed (NH_4^+ adducts are to the right of each peak); however, no PNA/DNA complexes exist. In Figure 3b, when P-Fl is combined with the complementary DNA duplex, C_A/C_B, multiple charge states

(52) Egholm, M.; Christensen, L.; Dueholm, K. L.; Buchardt, O.; Coull, J.; Nielsen, P. E. *Nucleic Acids Res.* **1995**, *23*, 217.
(53) Francois, J.-C.; Saison-Behmoaras, T.; Thuong, N. T.; Helene, C. *Biochemistry* **1989**, *28*, 9617.
(54) Hanvey, J. C.; Shimizu, M.; Wells, R. D. *Nucleic Acids Res.* **1990**, *18*, 157.
(55) Egholm, M.; Buchardt, O.; Nielsen, P. E.; Berg, R. H. *J. Am. Chem. Soc.* **1992**, *114*, 1895.
(56) Egholm, M.; Nielsen, P. E.; Buchardt, O.; Berg, R. H. *J. Am. Chem. Soc.* **1992**, *114*, 9677.
(57) Hanvey, J. C.; Peffer, N. J.; Bisi, J. E.; Thomson, S. A.; Cadilla, R.; Josey, J. A.; Ricca, D. J.; Hassman, C. F.; Bonham, M. A.; Au, K. G.; Carter, S. G.; Bruckenstein, D. A.; Boyd, A. L.; Noble, S. A.; Babiss, L. E. *Science* **1992**, *258*, 1481.
(58) Nielsen, P. E.; Egholm, M.; Berg, R. H.; Buchardt, O. *Nucleic Acids Res.* **1993**, *21*, 197.
(59) Nielsen, P. E.; Christensen, L. *J. Am. Chem. Soc.* **1996**, *118*, 2287.
(60) Wittung, P.; Nielsen, P.; Nordén, B. *Biochemistry* **1997**, *36*, 7973.
(61) Demidov, V. V.; Frank-Kamenetskii, M. D. *Methods* **2001**, *23*, 108.

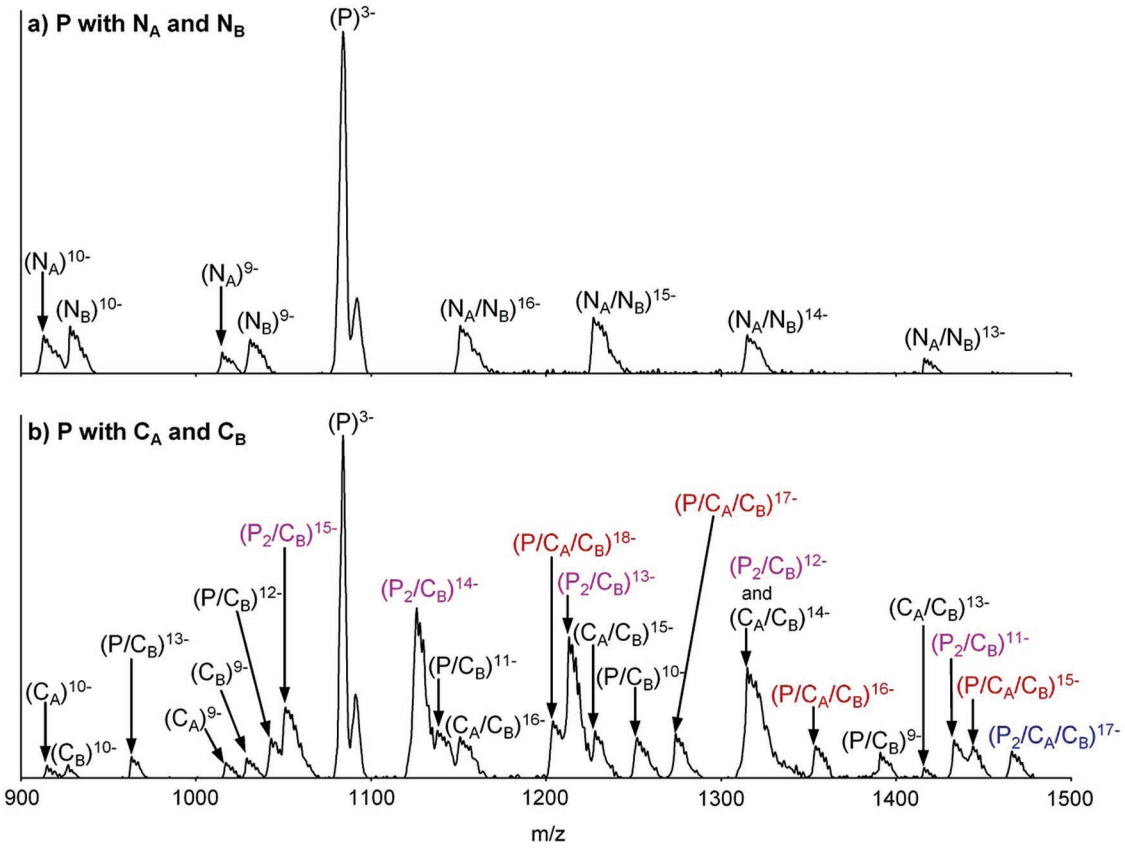

Figure 3. Nano-ESI mass spectra of P-Fl in a 15 to 1 excess over the (a) noncomplementary 30 bp duplex N_A/N_B and (b) complementary 30 bp duplex C_A/C_B. $(P\text{-Fl})_2/C_B$ complexes are shown in pink, $P\text{-Fl}/C_A/C_B$ complexes are red, $(P\text{-Fl})_2/C_A/C_B$ is blue, and all single and double-strands are black. Because of space constraints, P corresponds to P-Fl in the peak designation scheme.

of a variety of different complexes result including $P\text{-Fl}/C_B$, $(P\text{-Fl})_2/C_B$, $P\text{-Fl}/C_A/C_B$, and $(P\text{-Fl})_2/C_A/C_B$. Comparing these two mass spectra illustrates the highly selective nature of PNA/DNA binding, as nonspecific two-, three-, and four-stranded complexes are not present. We can also infer that the weak FRET emission observed for the 15:1 $P\text{-Fl}/N_A/N_B$ is based on hydrophobic interactions between PFP and P-Fl. In contrast, the FRET observed in the 15:1 $P\text{-Fl}/C_A/C_B$ solution is due to the presence of P-Fl binding to both C_B and C_A/C_B.

A significant amount of the three-strand complexes $(P\text{-Fl})_2/C_B$ and $P\text{-Fl}/C_A/C_B$ are observed in the mass spectrum, while only one band for higher-order complexes occurs in the gel. When analyzing the complexes in the gel, N_A/N_B, C_A/C_B, and $P\text{-Fl}/C_B$ duplexes all have similar migration rates, thereby indicating that replacing a 30-base DNA strand with a 10-base P-Fl does not affect the migration of the complexes to an appreciable extent. From this, it is reasonable to assume that $(P\text{-Fl})_2/C_B$ and $P\text{-Fl}/C_A/C_B$ might have similar migration rates and that the band for the higher-order complex could be a combination of both $(P\text{-Fl})_2/C_B$ and $P\text{-Fl}/C_A/C_B$. A $(P\text{-Fl})_2/C_A/C_B$ complex was also observed in the mass spectrum, but the low abundance of this complex would result in a very weak band (i.e., not visible) in the gel.

Ion Mobility. The binding site specificity of P-Fl and the conformational properties of the PNA/DNA complexes were examined with ion mobility experiments. ATDs (300 K) for each charge state of $P\text{-Fl}/C_B$, $(P\text{-Fl})_2/C_B$, $P\text{-Fl}/C_A/C_B$, and $(P\text{-Fl})_2/C_A/C_B$ were collected. In each case the number of ATD peaks agree for all charge states, so only the lowest charge state ATDs are shown in Figure 4. A single ATD peak was detected for all charge states of $P\text{-Fl}/C_B$, indicating that only one family of conformers is present (Figure 4a). However, two peaks were observed for $(P\text{-Fl})_2/C_B$, $P\text{-Fl}/C_A/C_B$, and $(P\text{-Fl})_2/C_A/C_B$ (Figure 4b−d), and because the ions are mass filtered after the drift cell, the two peaks must represent significantly different conformations. Experimental cross sections for each complex were calculated and an interesting trend was observed. As the charge state of each complex becomes more negative, an enlargement in cross section of 1−2% per charge state results (Table 1 and Figure 5a). While this enlargement is likely due to an increase in charge repulsion between the strands, theoretical modeling was employed to investigate this trend.

To identify the experimental conformation of the single ATD peak observed for $P\text{-Fl}/C_B$, a specifically bound duplex with P-Fl WC bound to the complementary region of C_B and the unpaired ends of C_B extending above and below the double-stranded region was used as the starting structure for 300 K dynamics simulations. A single steady state was observed in the dynamics plot of cross section versus time (Figure 5a) for each charge state of $P\text{-Fl}/C_B$, and the cross section increased 1−2% per charge state, similar to the experimental trend. When the resulting $P\text{-Fl}/C_B$ duplex structures were analyzed (Figure 4a), P-Fl remains WC bound to the complementary region in the center of C_B, all of the 10 WC base pairs remain intact, and the unbound ends of C_B fold down around the duplex region. The only structural variation observed was an extension of C_B for the more negative charge states due to increased charge repulsion, which accounts for the enlargement in cross section. When these cross sections were compared to the experimental

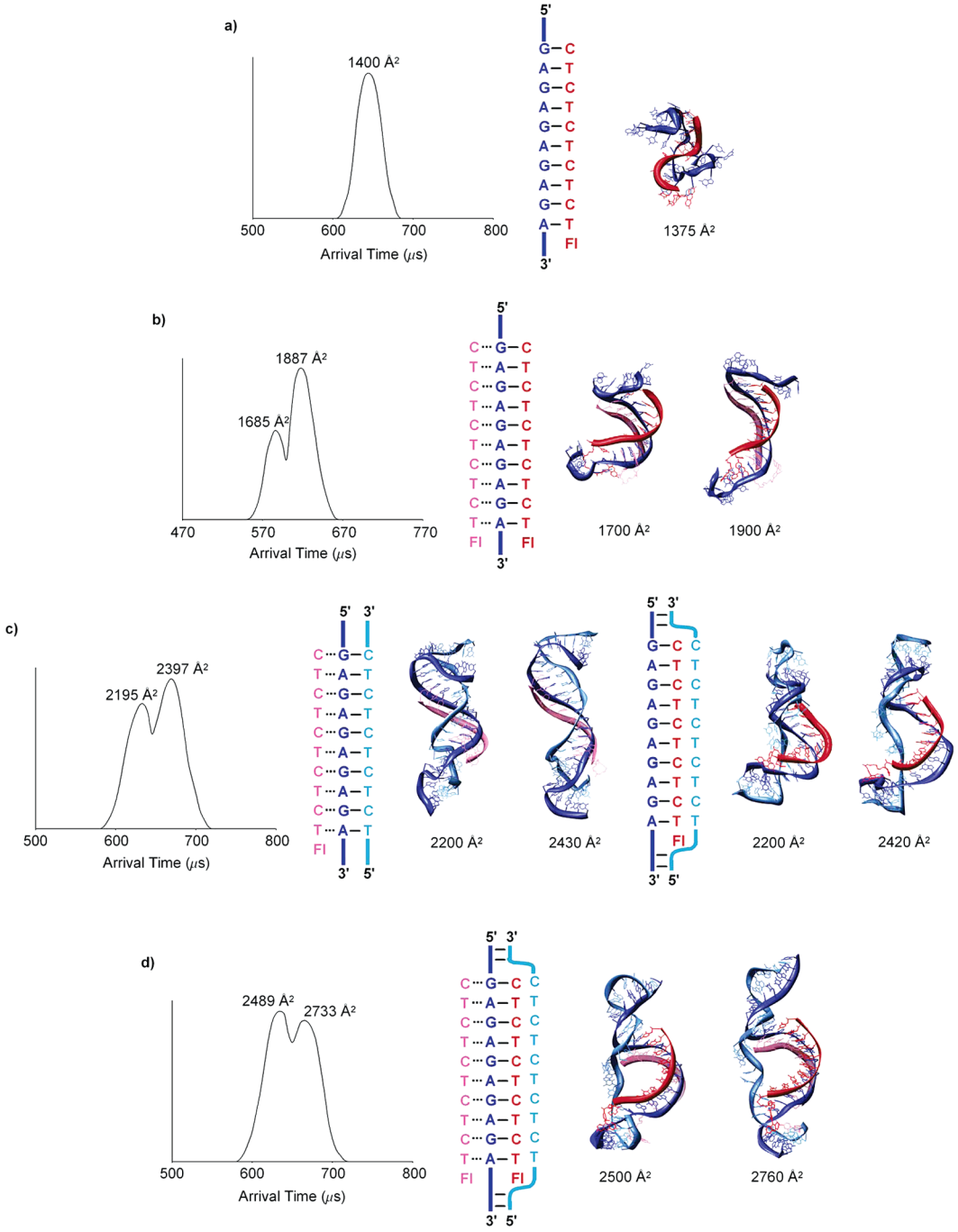

Figure 4. For each complex, ATDs are shown on the left, a schematic of the complex is shown in the center, and theoretical structures are shown on the right. C_A is shown in light blue, C_B is shown in dark blue, WC bound P-Fl is shown in red, and Hoogsteen-bound P-Fl is shown in pink. A single conformer is observed for (a) $[P\text{-}Fl/C_B]^{9-}$ and two conformers are present for (b) $[P\text{-}Fl/C_A/C_B]^{11-}$, (c) $[P\text{-}Fl/C_A/C_B]^{15-}$ (triplex (center) and duplex invasion (right)), and (d) $[(P\text{-}Fl)_2/C_A/C_B]^{17-}$.

cross sections, they agreed within 2% (Table 2), indicating that experimentally P-Fl/C_B had a specifically bound duplex conformation.

Since it was observed for the P-Fl/C_B duplex that increasing the strand repulsion simply causes the conformation to enlarge slightly (Figure 5a), only the lowest charge states of the specifically bound complexes for $(P\text{-}Fl)_2/C_B$, P-Fl/C_A/C_B, and $(P\text{-}Fl)_2/C_A/C_B$ will be discussed. A specifically bound PNA_2/DNA triplex, where one P-Fl is WC bound to C_B and the other P-Fl is Hoogsteen bound to C_B, was used as the starting structure for $[(P\text{-}Fl)_2/C_B]^{11-}$. Two steady states at 1700 and 1900 Å^2 were observed in the dynamics of the triplex as shown in Figure 5b, and a representative structure at each steady state is shown in Figure 4b. In both of the conformers, the unpaired ends of C_B collapse around the triplex region similar to the unpaired ends in the P-Fl/C_B duplex. However, in the smaller conformer, the triplex bends to form a more compact structure. Comparison between the experimental and theoretical cross sections indicated that the smaller conformer correlates within 2% of the cross section for the shortest time ATD peak, while the larger conformer agrees with the longest time peak (Table 2).

For P-Fl/C_A/C_B, both a specifically bound PNA/DNA_2 triplex and a PNA/DNA_2 duplex invasion complex (Scheme 4b and c) are possible conformations, so theoretical modeling was per-

Table 1. Experimental Cross Sections (Å^2) of the PNA/DNA Complexes versus Charge State[a]

complex	charge state				
	x	$x-1$	$x-2$	$x-3$	$x-4$
P-Fl/C_B[b]	1400	1419	1441	1462	1484
$(P\text{-}Fl)_2/C_B$[c]	1685	1710	1744	1761	1784
	1887	1903	1934	1964	1990
P-Fl/C_A/C_B[d]	2195	2231	2264	2290	
	2397	2436	2466	2497	
$(P\text{-}Fl)_2/C_A/C_B$[e]	2489				
	2733				

[a] 1% reproducibility error. [b] x = −9. [c] x = −11. [d] x = −15. [e] x = −17.

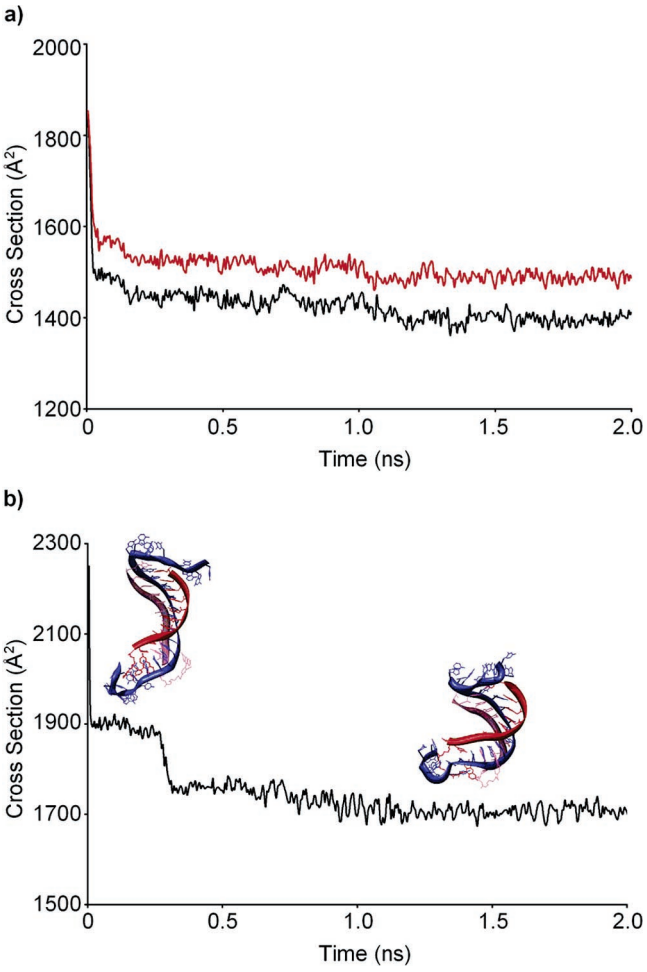

Figure 5. Plots of cross section versus dynamics time for (a) the −9 (black) and −13 (red) charge states of the P-Fl/C_B duplex and (b) the $[(P\text{-}Fl)_2/C_B]^{11-}$ triplex. Dynamics simulations were run at 300 K for 2 ns, and every 5 ps a structure was saved and its cross section calculated. Only one steady state was observed for the P/C_B duplexes; however, the −13 charge state has a larger cross section due to increased charge repulsion. Two steady states occur for the $[(P\text{-}Fl)_2/C_B]^{11-}$ triplex.

formed on both. The P-Fl/C_A/C_B triplex, where P-Fl is Hoogsteen bound to the C_A/C_B duplex (Figure 4c, left), was analyzed first. During the 300 K dynamics of the $[P\text{-}Fl/C_A/C_B]^{15-}$ triplex, two steady states at 2200 and 2430 Å^2 resulted and a representative structure at each steady state is shown in Figure 4c. In the larger conformer, the DNA duplex ends are more extended from the triplex region, while the duplex ends in the smaller conformer collapse around the triplex region, resulting in a more compact structure. Next, the P-Fl/C_A/C_B duplex invasion

Table 2. Experimental and Theoretical Cross Sections (Å^2) of the PNA/DNA Complexes (only the lowest charge state of each complex is illustrated)

complex	expt[a]	theory[b]	
		specific PNA binding	nonspecific PNA binding
$[P\text{-}Fl/C_B]^{9-}$	1400	1375	1305
$[(P\text{-}Fl)_2/C_B]^{11-}$	1685, 1887	1700, 1900	1620
$[P\text{-}Fl/C_A/C_B]^{15-}$	2195, 2397	2200, 2430 (Hoog)[c]	2095
		2200, 2420 (WC)[c]	
$[(P\text{-}Fl)_2/C_A/C_B]^{17-}$	2489, 2733	2500, 2760	2350

[a] 1% reproducibility error. [b] ≤2% standard deviation. [c] In P-Fl/C_A/C_B, P-Fl can either Hoogsteen (Hoog) or WC bind to the complementary region.

complex was studied. For this complex, the P-Fl strand invades the C_A/C_B duplex, and WC binds to C_B, in turn causing C_A to form a D-loop around the P-Fl/C_B duplex region (Figure 4c, right). Two steady states at 2200 and 2420 Å^2 occur in the dynamics plot for the $(P\text{-}Fl/C_A/C_B)^{15-}$ duplex invasion complex, where the DNA duplex ends extend out from the P-Fl/C_B duplex region in the larger conformer and collapse around the P-Fl/C_B region in the smaller conformer. The P-Fl/C_B duplex region in the smaller conformer also bends more than the larger conformer, causing a smaller, more compact structure. Unfortunately, the conformers of the triplex and duplex invasion complexes have almost identical cross sections so that, even though they both agree with the experimental cross sections as shown in Table 2 (the smallest conformers agree with the cross section for the shortest time peak, whereas the largest conformers match the longest time peak), calculating the percentage of each is impossible. Thus, the ATD for $[P\text{-}Fl/C_A/C_B]^{15-}$ contains either the triplex or the duplex invasion complex or a mixture of both, but due to the similarities in size, the percentage of triplex and duplex invasion complexes cannot be quantified.

The final complex for analysis was $(P\text{-}Fl)_2/C_A/C_B$ which was present in small amounts as shown in the mass spectrum (Figure 3b, $[(P\text{-}Fl)_2/C_A/C_B]^{17-}$). To identify the conformations of $[(P\text{-}Fl)_2/C_A/C_B]^{17-}$ a specifically bound triplex invasion complex was studied. In the starting triplex invasion complex, one P-Fl WC binds to C_B, another P-Fl Hoogsteen binds to C_B causing C_A to form a D-loop around the triplex region (Figure 4d). Two steady states occur in the $[(P\text{-}Fl)_2/C_A/C_B]^{17-}$ triplex invasion complex at 2500 and 2760 Å^2, and a representative structure of each steady state is shown in Figure 4d. In the larger conformer, the DNA duplex ends extend away from the $(P\text{-}Fl)_2/C_B$ triplex region, while the smaller conformer's duplex ends collapse around the triplex region. The $(P\text{-}Fl)_2/C_B$ triplex region in the smaller conformer also bends more than the larger conformer, causing a smaller, more compact structure. These theoretical cross sections both correlate with the experimental cross sections (Table 2), where the shortest time ATD peak matches the smallest conformer, while the longest time peak agrees with the larger conformer.

Nonspecifically bound complexes were also modeled for P-Fl/C_B, $(P\text{-}Fl)_2/C_B$, P-Fl/C_A/C_B, and $(P\text{-}Fl)_2/C_A/C_B$ to ensure that P-Fl is actually binding to its complementary region of C_B. To generate nonspecific complexes, P-Fl was placed next to different noncomplementary regions of C_B or C_A/C_B (depending on the complex), allowing only a few WC or Hoogsteen pairs to form, in addition to many nonspecific hydrogen bonds. When 300 K dynamics simulations were performed on each nonspe-

cific complex, only one steady state, similar to the dynamics plot shown in Figure 5a, was observed. The resulting conformers were globular and too small to agree with the experimental cross sections (Table 2). Additionally, analysis of each charge state of the nonspecifically bound structures resulted in no change in the cross section compared to the 1−2% size increase observed in the experimental and specifically bound cross sections.

Summary

A homogeneous sensory scheme was designed for the specific detection of dsDNA. Using a water-soluble cationic conjugated polymer as the donor and a dye-labeled PNA as the acceptor, FRET experiments confirm specific PNA/dsDNA binding by a positive (acceptor) signal with complementary dsDNA. With complementary dsDNA, a number of complexes are possible. Gel electrophoresis, mass spectrometry, ion mobility, and molecular dynamics calculations were utilized in determining the types of complexes formed. Gel electrophoresis verified that at least one higher-order (three- or four-strand) complex was formed. Mass spectrometry was able to show that only sequence-specific binding of PNA to ssDNA and dsDNA occurs in solution, and it also provided evidence that specific three- and four-strand complexes were present. Finally, ion mobility in conjunction with molecular dynamics calculations confirmed only sequence-specific binding in the complementary region for all PNA/DNA complexes, while refuting the possibility of nonspecific binding. From these results, it could be concluded that PNA labeled with a fluorescent dye in conjunction with a water-soluble conjugated polymer allows for specific, direct detection of dsDNA without denaturing due to the ability of PNA to form three- and four-stranded complexes with DNA duplexes.

Acknowledgment. We gratefully acknowledge the support of the National Science Foundation under Grants CHE-0503728 (M.T.B.) and DMR-0097611(G.C.B.) and the National Institute of Health under Grants A1065359 and GM62958-01 (G.C.B.). Useful discussions with Michelle Massie and Prof. Stuart Feinstein are also gratefully acknowledged.

Supporting Information Available: The full citation for ref 41 and data for the other ratios of P-Fl to dsDNA. This material is available free of charge via the Internet at http://pubs.acs.org.

JA060069S